ACS OMEGA

Open Access

http://pubs.acs.org/journal/acsodf

Article

Intercalation of C60 into MXene Multilayers: A Promising Approach for Enhancing the Electrochemical Properties of Electrode Materials for High-Performance Energy Storage Applications

Hassan Bukhari, Asad M. Iqbal, Saif Ullah Awan,* Danish Hussain, Saqlain A. Shah, and Syed Rizwan

Cite This: *ACS Omega* 2024, 9, 227−238

Read Online

ACCESS | Metrics & More | Article Recommendations

ABSTRACT: In this study, we report on the enhancement of the electrochemical properties of MXene by intercalating C60 nanoparticles between its layers. The aim was to increase the interlayer spacing of MXene, which has a direct effect on capacitance by allowing the electrolyte flow in the electrode. To achieve this, various concentrations of Ti_3SiC_2 (known as MXene) and C60 nanocomposites were prepared through a hydrothermal process under optimal conditions. The resulting composites were characterized by using X-ray diffraction, scanning electron microscopy, energy dispersive spectroscopy, Raman spectroscopy, and cyclic voltammetry. Electrodes were fabricated using different concentrations of MXene and C60 nanocomposites, and current−voltage (I−V) measurements were performed at various scan rates to analyze the capacitance of pseudo supercapacitors. The results showed the highest capacitance of 348 F g^{1-} for the nanocomposite with a composition of 90% MXene and 10% C60. We introduce MXene-C60 composites as promising electrode materials for supercapacitors and highlight their unique properties. Our work provides a new approach to designing high-performance electrode materials for supercapacitors, which can have significant implications for the development of efficient energy storage systems.

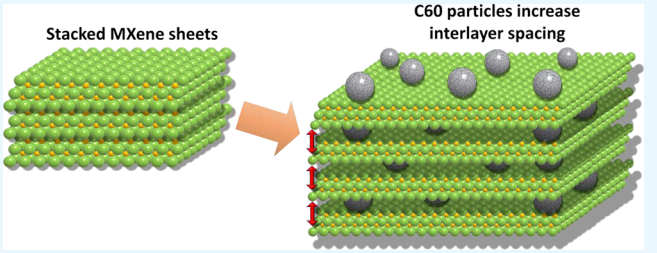

1. INTRODUCTION

Energy storage devices (ESDs) have become increasingly important in recent years due to the growing demand for renewable energy sources and the need for efficient energy storage systems. ESDs play a vital role in storing and supplying energy from various sources to electronic appliances. The choice of ESD depends on the specific application requirements, which include storage capacity, specific power, specific energy, reaction time, efficiency, lifetime, thermal resistivity, and cost. There are different types of ESDs, including batteries, fuel cells, standard capacitors, and supercapacitors.[1−6] Supercapacitors have emerged as a promising energy storage solution due to their high power density, which enables them to deliver a large amount of energy in a very short time. They exhibit short charging and discharging times, making them ideal for devices where fast energy transfers are required such as electric vehicles. Apart from high power density, supercapacitors possess long life cycles and are space efficient, lightweight, easy to handle, reliable, and compatible with other electronic components.[7−12]

There are two main types of supercapacitors that are commonly used, namely, electric double layer capacitors (EDLCs) that use a high surface area carbon electrode and an electrolyte to store charge. It has a relatively low voltage rating but can store a large amount of energy.[13−16] The second type is pseudo capacitors, which have the ability to store additional charge due to the specific electrode material that can undergo reversible redox reactions at the electrode surface. This allows them to store more energy than EDLCs and have a higher voltage rating.[17−20] Overall, supercapacitors have the potential to revolutionize the energy storage industry and be used in a wide range of applications. However, there are still challenges to be overcome, such as improving their energy density and reducing their cost before they can become a viable alternative to traditional batteries.[5,21−23] Supercapacitors are typically made with thin-film electrode materials in the shape of fibers or flat sheets, with or without soft-matter substrates for support.[24−26] Many nanostructured materials are frequently used in supercapacitors as electrode materials with improved performance, including carbon nanotubes, hierarchically porous carbon, and hollow metal oxides/sulfides. However, there are few electrode materials that can have both high volumetric and gravimetric specific capacitance.[27,28]

Received: June 8, 2023
Accepted: October 9, 2023
Published: December 28, 2023

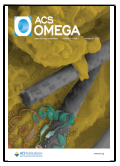

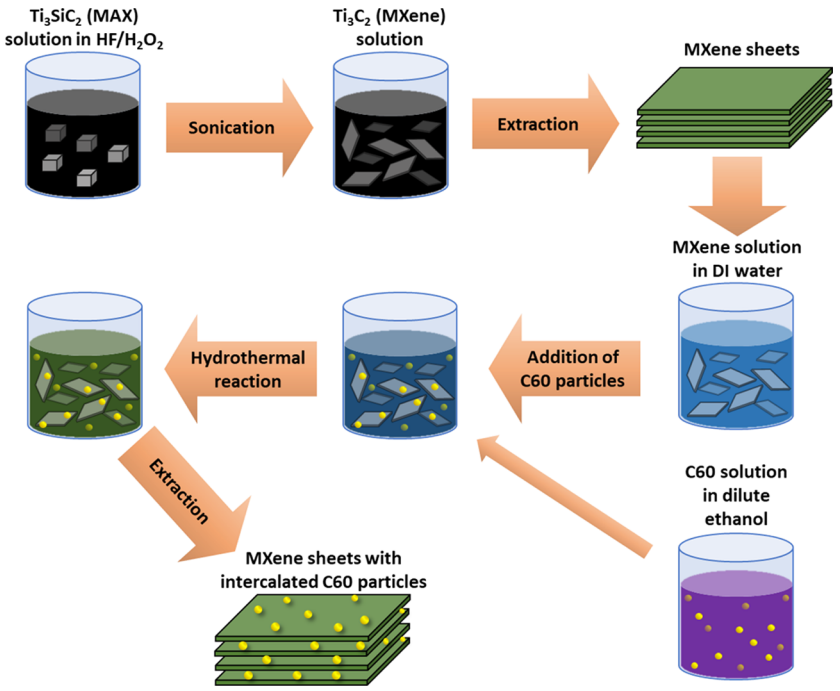

Figure 1. Experimental synthesis setup for the fabrication of MXene-C60 nanocomposites.

MXene, a new two-dimensional (2D) material, has recently emerged as a promising electrode material for supercapacitors due to its unique properties. MXenes consist transition metal carbides or nitrides that are produced through a process of selective etching of MAX (M = early transition metal, A = group A element, and X = carbon or nitrogen) phases. MXene has a layered structure with each layer consisting of transition metal atoms sandwiched between two carbon or nitrogen layers. The layers are held together by weak van der Waals forces, which allows them to be easily peeled off and stacked to form thin films or nanosheets. MXene exhibits a range of interesting properties, such as high electrical conductivity, high mechanical strength, and high surface area, which make it suitable for a wide range of applications. Especially the high surface area of MXenes allows for high capacitance, and their high electrical conductivity ensures efficient charge transport.[29−35] In addition, the interlayer spacing between MXene sheets can be tuned, providing additional opportunities to enhance their electrochemical properties, which makes it a potential candidate to be used as supercapacitor electrode.[36−40] C60, a spherical fullerene molecule made of 60 carbon atoms, has also been widely studied for its unique properties, including high surface area, chemical stability, and electrical conductivity.[41−46] Combining MXene and C60 can provide a new approach to improve the interlayer spacing of MXene and enhance its electrochemical properties.

In this paper, we aim to prepare MXene-C60 composites with different compositions and investigate the effect of interlayer spacing on the electrochemical properties of the composites. Ti_3C_2 MXene was prepared by etching the Ti_3SiC_2 MAX phase, and then C60 and MXene composites were formed through hydrothermal reaction and characterized through several techniques before using them to fabricate the electrode for supercapacitor device. Our results show that the composite with a composition of 90% MXene and 10% C60 exhibited the highest capacitance among all the composites studied. Overall, our results confirm that C60 intercalation enhances the electrochemical properties of MXene, making it a promising candidate for high-performance supercapacitor applications.

2. EXPERIMENTAL PROCEDURES

2.1. Methods and Materials. Ti_3C_2 MXene was obtained by etching Ti_3SiC_2 MAX powder in an HF/H_2O_2 solution. To prepare the etchant solution, 45 mL of HF was mixed with 5 mL of H_2O_2 in a 250 mL polypropylene bottle. Next, 3 g of Ti_3SiC_2 powder was added to the etchant solution, and the mixture was placed in an oil bath preheated to 55 °C. The solution was kept at this temperature with constant stirring (500 rpm using a 2 cm-long Teflon magnetic stirring bar) for 45 h to ensure complete removal of Si atoms from the MAX phase. After the reaction was complete, the product was washed repeatedly with deionized water and centrifuged at 5000 rpm. The resulting sample was then filtered by using a vacuum filtration setup to obtain a 2D layered Ti_3C_2 MXene structure. To separate the layers of MXene, a delamination process was used, in which tetramethyleammonium hydroxide (TMAOH) was added to the obtained product, and the mixture was heated to 55 °C with continuous magnetic stirring for 24 h. The mixture was then filtered to obtain the final product, i.e., 2D delaminated sheets of Ti_3C_2 MXene. Composites of MXene and C60 were prepared through a hydrothermal process in which commercially available C60 was used without any further purification. Solutions of MXene and C60 were prepared in deionized water and dilute ethanol, respectively. Both solutions were dispersed in a sonication bath for 30 min. The dispersed solution was transferred to a Teflon beaker and placed inside an autoclave, which was then kept in an oven at 90 °C for 24 h to carry out the hydrothermal process. To separate the solvents from the material, vacuum filtration with a filter paper of 0.22 μm pore size was used. However, the filtered powder still had some amount of solvent in it. To completely dry the obtained nanocomposites, the filter paper containing the nanocomposite on its surface was

https://doi.org/10.1021/acsomega.3c04058
ACS Omega 2024, 9, 227−238

left inside the vacuum drying chamber at 100 °C for 24 h. After the mixture was dried, MXene-C60 nanocomposites were obtained. Five samples of MXene-C60 composites were made with compositions; 10% MXene +90% C60 (S-1), 25% MXene +75% C60 (S-2), 50% MXene +50% C60 (S-3), 75% MXene +10% C60 (S-4), and 90% MXene +10% C60 (S-5), which were used for further characterizations. A schematic representation of the synthesis steps is shown in Figure 1.

The process involves several steps, such as the preparation of MXene through etching the MAX solution, the addition of the C60 particles to the MXene solution, and sonication to achieve a uniform dispersion. Finally, the composite material is obtained through vacuum filtration and drying.

2.2. Fabrication of Electrode for Supercapacitors. The method used to fabricate the electrode for a supercapacitor is crucial in determining its performance. The production phases, such as mixing, casting, spreading, and solvent evaporation, all affect the final attributes of the electrode.[47−50] Commonly used substrates for making electrodes include nickel foams, cobalt foams, and FTOs (fluorine-doped tin oxides).[51−53] In the present work, we used nickel foam as a substrate for making the MXene-C60 composite electrode. Prior to electrode fabrication, the substrate was washed in ethanol and DI water for 10 min each in a sonication bath and then dried at 55 °C on a hot plate. To prepare the slurry paste, we mixed 80% of MXene-C60 composite, 10% carbon black, 10% PVDF polyvinylidene difluoride (a highly nonreactive thermoplastic fluoropolymer), and 2 drops of NMP (*N*-methyl-2-pyrrolidone). Once all components of the slurry paste were mixed, it was sprayed onto the nickel foam using a spray gun and then kept inside a vacuum drying chamber at 100 °C for 24 h. A pressure of 5 psi was applied by a hydraulic press to distribute all components of the slurry paste uniformly, which was then used for electrochemical characterization. It is worth noting that the use of carbon black in the electrode composition helps to enhance the electrical conductivity of the electrode, while PVDF acts as a binder to hold the electrode material together.[50,54,55] In addition, the use of NMP as a solvent in the slurry paste aids in the uniform distribution of the electrode material on the substrate.

2.3. Characterization Techniques. The experimental tools utilized in this study to investigate the intercalation of C60 into MXene layers included X-ray diffraction (XRD), scanning electron microscopy (SEM), energy-dispersive X-ray spectroscopy (EDX), Raman spectroscopy, and cyclic voltammetry (CV). XRD was employed to identify the crystal structures and purity of the prepared samples. SEM analysis allowed for the investigation of the morphology of the intercalated MXene layers and the uniform distribution of C60. EDX was utilized to confirm the presence of C60 in the intercalated MXene layers and determine the elemental composition of the samples. Raman spectroscopy provided information about the structural changes that occurred as a result of the intercalation of C60 into the MXene layers. Finally, CV was used to measure the electrochemical performance of the intercalated MXene layers and compare it to the performance of the unmodified MXene layers. The XRD measurements were performed using a Bruker D8 Advance diffractometer with Cu Kα radiation (λ = 1.5406 Å) over a 2θ range of 5−80°. The SEM images were obtained using a JEOL 6490-A scanning electron microscope, and the EDX measurements were performed by using the same SEM instrument. Raman spectra were recorded by using a Horiba Scientific Explora One spectrometer. The CV measurements were performed using a Gamry Cyclic Voltameter Interface 1010E instrument with a three-electrode configuration. These experimental tools provided comprehensive characterization of the intercalated MXene layers and valuable insight into the structural and electrochemical changes that occurred as a result of the intercalation process.

3. RESULTS AND DISCUSSION

3.1. Structural Analysis. The X-ray diffraction (XRD) spectra of the MAX phase, MXene, and composite samples 1 and 3 are presented in Figure 2. The XRD spectrum of MAX

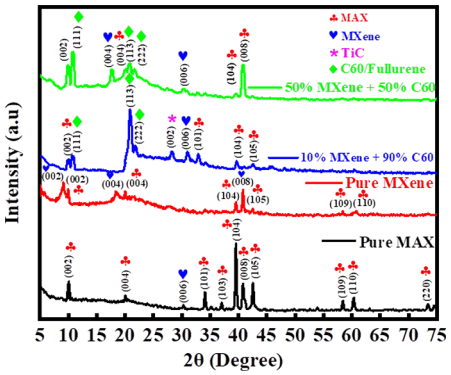

Figure 2. XRD pattern of MAX, MXene, 10% MXene +90% C60, and 50% MXene +50% C60 nanocomposites.

phase exhibits characteristic peaks at (002), (004), (006), (101), (103), (104), (008), (105), (108), (109), and (110), which are in agreement with the reported crystal planes for Ti_3SiC_2.[56−58] In contrast, the XRD spectrum of MXene shows only (002), (004), (006), and (008) peaks, indicating the formation of the desired 2D layered structure.[58−60] The composite samples display all of the peaks corresponding to the structures of C60 and MXene, indicating that both constituents do not react chemically and only form a composite, remaining in their characteristic structures without forming any impurity phase. The relative intensity of C60 peaks compared to that of MXene is high in sample 1 and decreases in sample 3, which is in accordance with the weight concentration of C60 in both of these samples. The XRD results suggest that the composites possess good crystallinity and confirm the successful synthesis of MXene-C60 composites through a hydrothermal process.

3.2. Morphology and Elemental Analysis. Figure 3a−d displays the surface morphology of C60 particles, revealing their characteristic spherical shape with an average grain size of approximately 30 μm. However, the roughness of the surface suggests that the particles are oxidized.[61,62] SEM images of MXene are presented in Figure 3e,f where the layered structure can be observed at some places; however, the remaining portion appears to be like bulk grains, which is due to the stacking or close packing of MXene layers with each other. SEM images of the composite sample with the composition 50% C60 + 50% MXene (Figure 3g−j) indicate a homogeneous distribution of MXene and C60, with no visible aggregation or agglomeration. Interestingly, the lining between MXene layer is more prominent in the composite sample as compared to that in pure MXene. This indicates successful intercalation of C60 particles between MXene layers, which

https://doi.org/10.1021/acsomega.3c04058
ACS Omega 2024, 9, 227−238

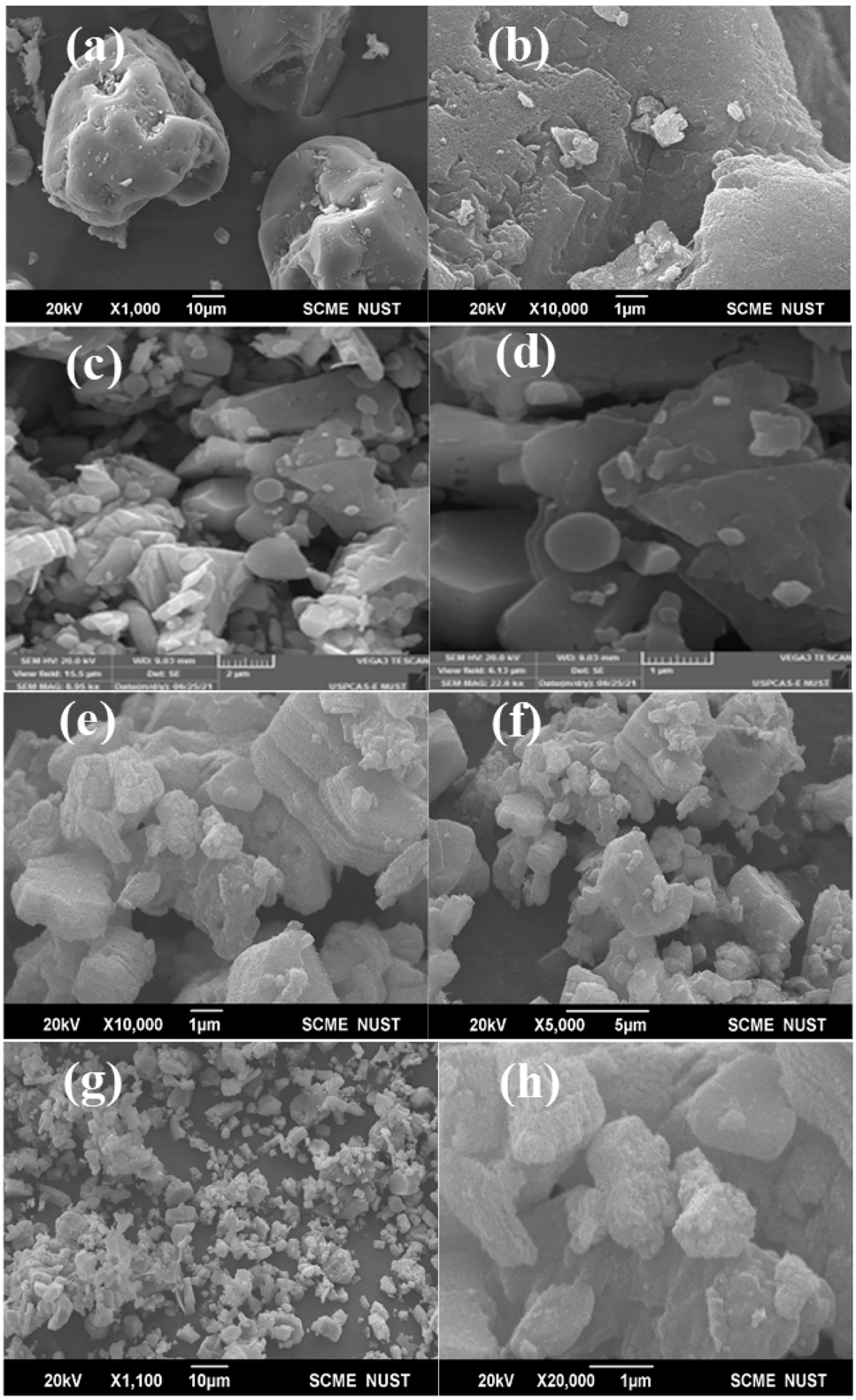

Figure 3. SEM images (a, b) C60, (c, d) MXene, and (e, h) MXene-C60 nanocomposite (50% MXene +50% C60).

cases an increase in the interlayer spacing. EDX analysis was conducted to analyze the elemental composition of C60 and the composite sample and is shown in Figure 4. The EDX spectrum of C60 shows a single peak corresponding to carbon. However, in the EDX spectrum of the composite sample, multiple peaks are observed, which are identified as titanium, carbon, silicon, fluorine, and oxygen. The presence of fluorine and oxygen can be attributed to the compounds used during the etching process, while the remaining peaks correspond to the MXene and MAX phases. Overall, SEM and EDX analyses confirmed the successful formation of the MXene-C60 composites with a homogeneous distribution of both

https://doi.org/10.1021/acsomega.3c04058
ACS Omega 2024, 9, 227−238

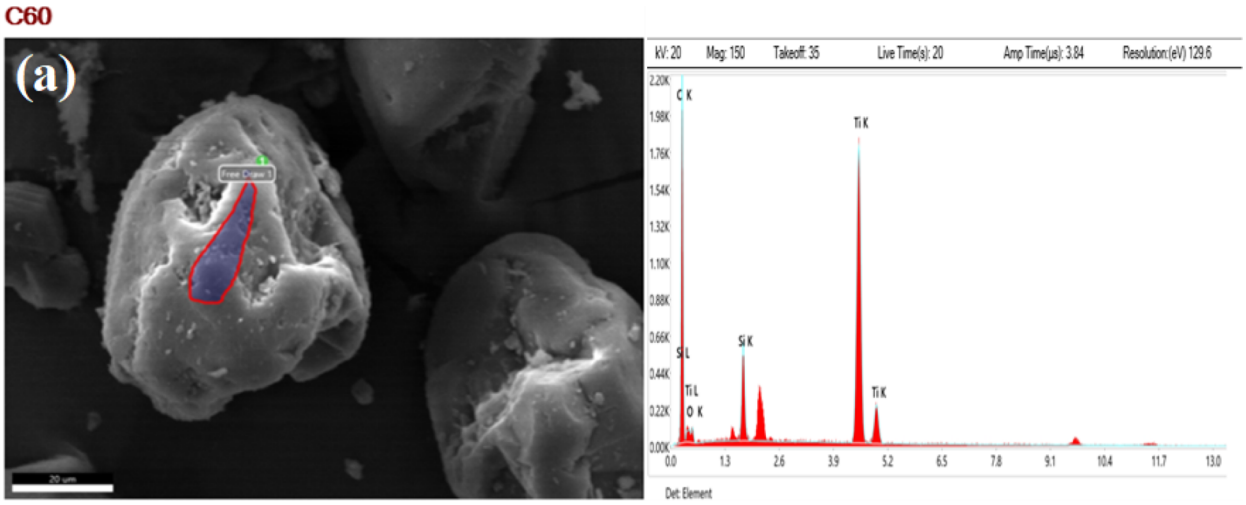

eZAF Quant Result - Analysis Uncertainty: 13.50 %				
Element	Weight %	MDL	Atomic %	Error %
C K	100.0	0.07	100.0	8.8

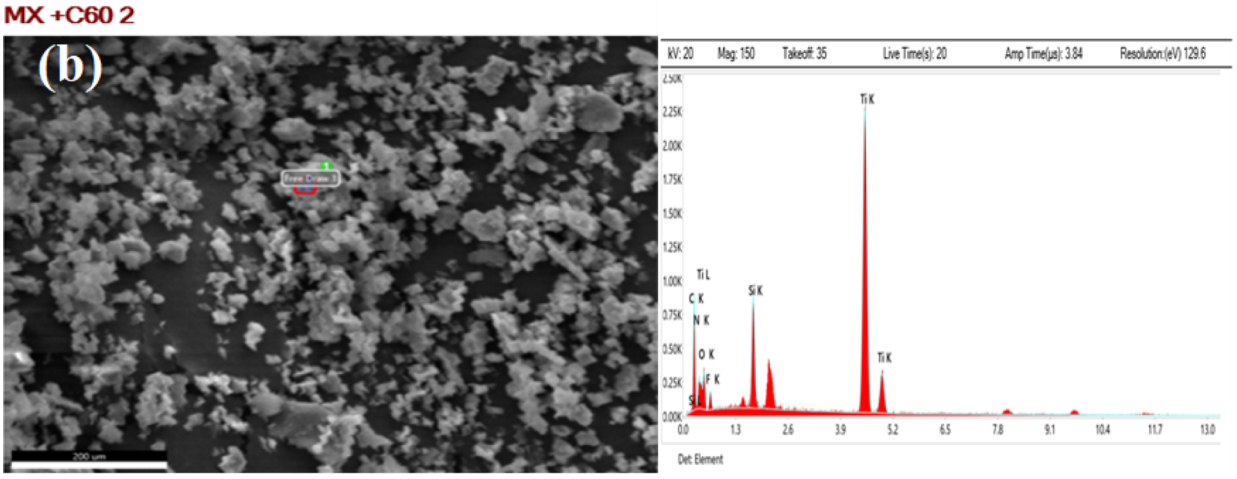

eZAF Quant Result - Analysis Uncertainty: 13.54 %				
Element	Weight %	MDL	Atomic %	Error %
C K	27.4	0.64	46.9	11.9
N K	2.9	1.91	4.3	31.0
O K	15.9	1.50	20.5	15.3
F K	5.2	0.73	5.7	16.6
Si K	6.0	0.15	4.4	6.8
Ti K	42.5	0.27	18.3	2.4

Figure 4. EDX spectrum: (a) C60; (b) MXene-C60 nanocomposite (50% MXene +50% C60).

constituents. These findings are consistent with the XRD analysis and further support the potential of Mxene-C60 composites as high-performance electrode materials for supercapacitor applications.

3.3. Raman Spectroscopy. Raman spectroscopy was used to study the vibrational modes of the intercalated MXene-C60 nanocomposites with varying compositions. The Raman spectra (Figure 5) showed peaks corresponding to both MXene and C60 materials, which exhibited a shift in peak positions and Raman shift with varying compositions. Specifically, the characteristic peaks of MXene were observed at 220 and 420 cm^{-1}, while those of C60 were observed at 1465 cm^{-1}. The variation in peak intensities was found to follow a nearly consistent trend with the change in

https://doi.org/10.1021/acsomega.3c04058
ACS Omega 2024, 9, 227−238

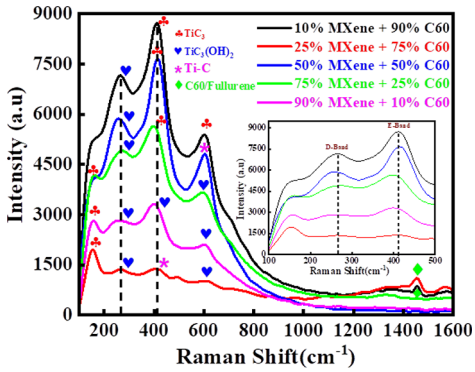

Figure 5. Raman spectrum of 10% MXene +90% C60, 25% MXene +25% C60, 50% MXene +50% C60, 75% MXene +25% C60, and 90% MXene +10% C60 nanocomposites.

composition, indicating the successful incorporation of C60 into the MXene layers. Notably, in MXene-rich compositions, peaks corresponding to C60 completely vanished, indicating that the C60 nanoparticles were effectively intercalated into the MXene layers.

3.4. Cyclic Voltammetry. sCyclic voltammetry was used to study the electrochemical behavior of the prepared composites using a three-electrode system in 6 M KOH as electrolyte. The cyclic voltammograms of all the samples at different scan rates in a potential window of 0.1 to 0.6 V are presented in Figures 6 and 7. MXenes have a layered structure that is partially delaminated, allowing both ion intercalation and EDLC formation to contribute to charge storage.[63,64] Especially, when acidic electrolytes (e.g., H_2SO_4) are used, distorted rectangular CV curves are observed because of the contribution from the Faradaic redox reactions.[65,66] The electrochemical behavior of MXenes is strongly influenced by the electrode fabrication procedure. A completely delaminated MXene should show different electrochemical behavior than that observed in stacked MXene nanosheets. Delamination of the nanosheets by sonication, which is frequently used to fabricate free-standing MXene films, alters the relative fraction of these two contributions to charge storage.[67−70] In the present work, the aim was to increase the interlayer spacing between MXene sheets through the process of the intercalation of C60 particles between the MXene sheets. Increased space between MXene layers enhances the diffusion of electrolyte into the electrode material, which gives rise to the high capacitance values for the material.

The cyclic voltammograms (CV) of the prepared composite samples showed EDLC behavior in the beginning and then a sharp rise in the current, which is due to the layered structure of MXene that allows ion diffusion and gives rise to the intercalation pseudo capacitance effects. The layered structure of MXene provides a path and increased surface area to the ions in the electrolyte for redox reactions. However, the curves show a strong dependence on scan rate, which occurs because, at higher scan rates, ions do not get enough time to travel into the layered electrode due to which the peak current decreases with an increase in scan rate. Furthermore, a consistent rise in the peak current was observed with the increase in MXene concentration in the composites (see Figure 6).

Figure 8 shows the capacitance as a function of MXene concentration in the composite for various scan rates where it can be seen that for each scan rate, the highest value of capacitance is observed for sample 5, which contains the highest concentration of MXene. Interestingly, the observed value of the capacitance for sample 5 (340 F g^{1-}) is higher than the previously reported capacitance for MXene (240 F g^{1-}). This confirms that the C60 particles were successfully induced between the MXene layers, which increased the interlayer spacing and allowed for the easy flow of electrolyte between the MXene layers. Furthermore, sample 5, which contains the highest MXene concentration, is the optimal composition for achieving high capacitance for supercapacitors.

3.5. Mechanism. Supercapacitors store energy through electrochemical pseudocapacitance and electrostatic double-layer capacitance (EDLC), both of which contribute to the total capacitance of the capacitor. The EDLCs use carbon electrodes that achieve separation of charge in a Helmholtz double layer at the interface between the surface of a conductive electrode and an electrolyte. The separation of charge is of the order of a few angstroms (3−8 Å), which is much smaller than in a conventional capacitor.[71−73] In contrast, pseudocapacitance is achieved by Faradaic electron charge transfer through redox reactions. Therefore, the surface area of the electrode available for redox reactions directly influences the magnitude of pseudocapacitance.[74−76]

MXene is a 2D material that has a large surface area, making it a potential candidate for use as an electrode material for supercapacitors. MXenes are known to exhibit pseudocapacitance due to the Faradaic redox reactions that occur at their surface.[77−79] The general reaction that could occur at the surface of a MXene electrode is

$$\mathrm{MXene}(M_{n+1}X_nT_n) + ne^- \rightleftharpoons \mathrm{MXene}(M_n + X_nT_{n+1})$$

where M represents a transition metal such as Ti, V, or Nb, X represents a carbon or nitrogen atom, T represents a surface termination such as O, OH, or F, n is the number of metal atoms in the MXene layer, and e^- represents an electron. In this reaction, n electrons are transferred per metal ion, leading to a change in the oxidation state of the metal. The reverse reaction occurs during the discharge process, where the stored charge is released. However, it is important to note that the specific redox reaction that occurs on the surface of a MXene electrode may depend on various factors such as the specific MXene composition, the type of electrolyte used, the applied potential, and the operating conditions of the supercapacitor. These reactions involve the transfer of electrons between the electrode material and electrolyte, leading to the formation of charged species on the surface of the electrode.

However, MXene layers are usually stacked with each other, which allows for a much less effective surface area for redox reactions. Therefore, increasing the interlayer spacing of MXene (either by varying the synthesis parameters, etchant solution or by making composites with other materials) is a useful way to increase the capacitance.[80−82] In the present work, C60 is used as intercalating particles that situate themselves between the MXene layers and therefore cause an increase in the interlayer spacing. The increased interlayer spacing allows more electrolyte for the redox reactions, resulting in an increase in capacitance. This mechanism is schematically depicted in Figure 9. The increased capacitance in our samples confirms that C60 particles have been successfully intercalated between the MXene layers and the interlayer spacing has been increased. It is essential to note that the highest capacitance is observed for the composition that contains 90% MXene and 10% C60. The capacitance consistently decreased as the concentration of C60 increased

https://doi.org/10.1021/acsomega.3c04058
ACS Omega 2024, 9, 227−238

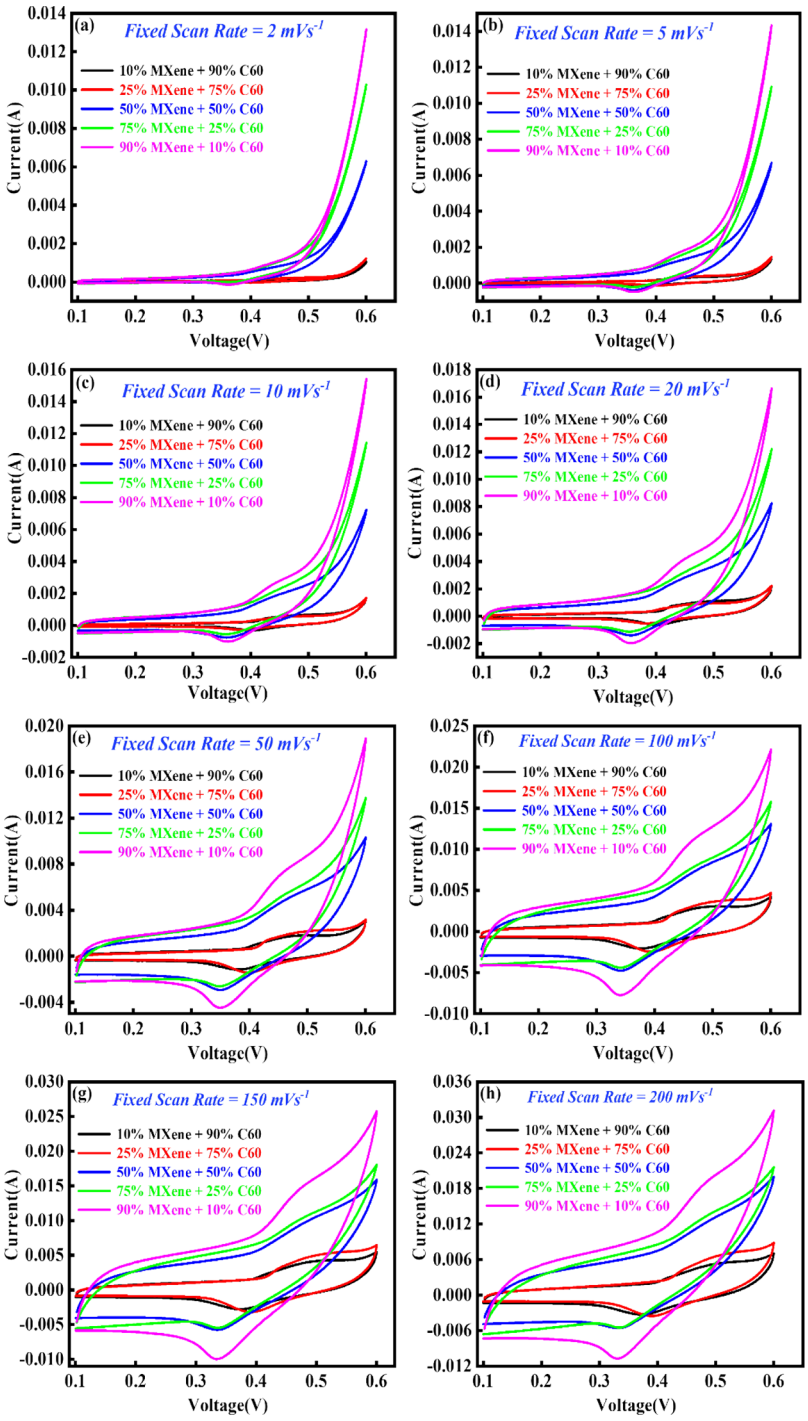

Figure 6. Cyclic voltammograms of all MXene-C60 nanocomposites at fixed scan rates: (a) 2, (b) 5, (c) 10, (d) 20, (e) 50, (f) 100, (g) 150, and (h) 200 mV s^{-1}.

in the sample. This finding can be attributed to the unique electrochemical properties of MXene, which contribute to its exceptional performance when used in energy storage devices. MXene, with its two-dimensional layered structure, provides a significantly large effective surface area, enabling abundant sites for redox reactions. Consequently, MXene exhibits high capacitance due to its enhanced charge storage capacity. To further elaborate, the key factor for MXene's exceptional capacitance lies in the accessibility of its interlayer spacing, allowing efficient electrolyte diffusion into the electrode material. By separating the MXene layers or increasing the interlayer spacing, the electrode facilitates the penetration of the electrolyte, enhancing ion mobility and enabling more effective charge storage. On the other hand, when C60 is employed solely as an electrode material, it predominantly exhibits EDLC behavior, similar to traditional carbon electrodes. In the present work, the role of C60 is to increase the interlayer spacing between the MXene sheets. However, as the concentration of C60 increases above 10% in the composite electrode, despite the expanded interlayer spacing, the overall capacitance decreases. This decline can be attributed to the reduced MXene content in the electrode, leading to a

https://doi.org/10.1021/acsomega.3c04058
ACS Omega 2024, 9, 227−238

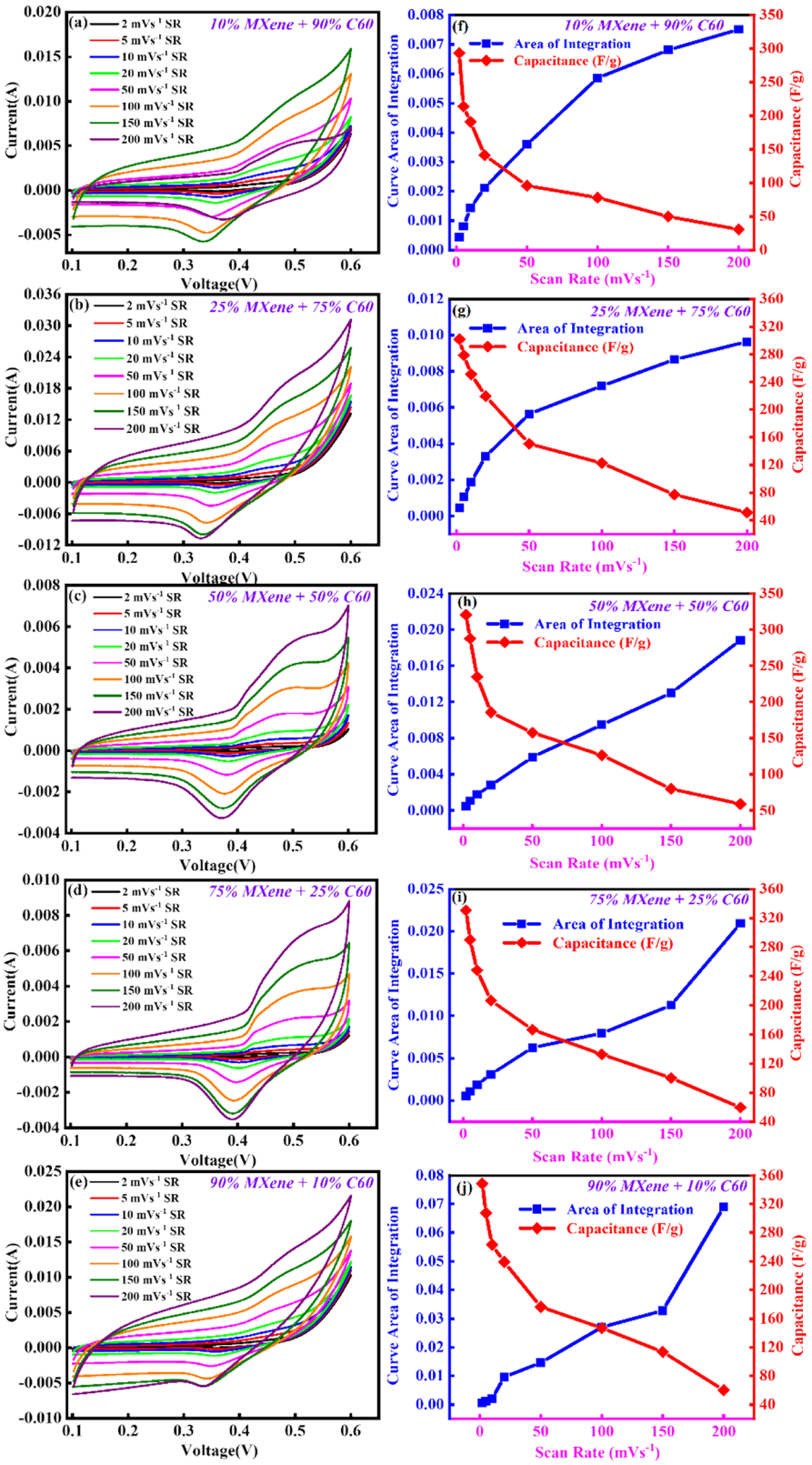

Figure 7. Cyclic voltammograms of all MXene-C60 nanocomposites at different scan rates: (a) 10% MXene +90% C60, (b) 25% MXene +25% C60, (c) 50% MXene +50% C60, (d) 75% MXene +25% C60, and (e) 90% MXene +10% C60. Area of integration and capacitance for all MXene-C60 nanocomposites versus different scan rates: (f) 10% MXene +90% C60, (g) 25% MXene +25% C60, (h) 50% MXene +50% C60, (i) 75% MXene +25% C60, (j) 90% MXene +10% C60.

diminished contribution from the high-capacitance MXene component. Consequently, the increase in C60 concentration outweighs the benefits of interlayer spacing, resulting in a decrease in the overall capacitance. Therefore, the optimal composition for the MXene-C60 composite electrode is 90% MXene and 10% C60. To further enhance the capacitance of

https://doi.org/10.1021/acsomega.3c04058
ACS Omega 2024, 9, 227−238

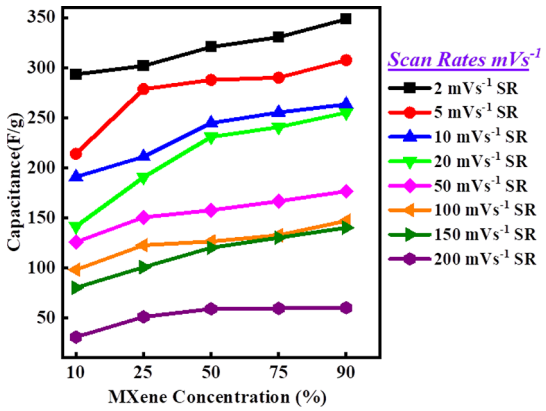

Figure 8. Capacitance of all MXene-C60 nanocomposites of different MXene concentrations at different scan rates.

the MXene-C60 composite electrode, more compositions need to be prepared with C60 concentration in the range of 0−20%. The capacitance can also be improved by increasing the interlayer spacing of MXene by altering the synthesis parameters or the etchant solution. Moreover, by introduction of other intercalating particles, the interlayer spacing can be further increased, leading to a higher capacitance.

To date, numerous different MXene materials have been successfully synthesized and characterized. The MXene family continues to expand, as researchers explore new combinations of transition metals and surface functionalization techniques. Each MXene material possesses unique properties and potential applications, making the field of MXene research dynamic and exciting.[83−90] However, as also discussed in the Introduction section, the major issue in MXenes is the easy restacking or agglomeration of MXene sheets, which hinders the mobility of the electrolyte between the layers and drastically affects electrochemical properties. Researchers have attempted various techniques to enhance the electrochemical properties of MXenes, such as modifying the etching solution or parameters,[91−93] implementing postsynthesis treatments like alkalinization,[94,95] and creating composites by combining MXene with other suitable materials.[96,97] Composites can improve properties in two ways. First, they can provide a conductive path for charge carriers, as seen with materials like carbon nanotubes or graphene.[89,98] Second, composites can prevent or reduce restacking or agglomeration of MXene layers.[99] In comparison to other MXenes and previous improvement methods, our study focused on investigating the impact of interlayer spacing on the electrochemical properties of MXene and C60 composites. C60 was utilized to increase the interlayer spacing of the MXene layers. Our findings demonstrate that the addition of C60 successfully increased the interlayer spacing, showcasing the effectiveness of this approach in enhancing the energy storage capabilities of MXene-based electrode materials. Moreover, the composite with a composition of 90% MXene and 10% C60 exhibited the highest capacitance among all of the composites studied. These findings contribute to a more comprehensive understanding of the phenomena under study and highlight the potential of interlayer spacing manipulation using C60 for the development of efficient energy storage systems.

In conclusion, we have successfully synthesized Mxene-C60 composites through a facile solvothermal method. The XRD analysis confirms that C60 particles have been intercalated between the MXene layers, leading to an increase in interlayer spacing. The electrochemical characterization of the composites showed that the intercalation of C60 particles significantly improves the capacitance of MXene-based supercapacitors by increasing the interlayer spacing, allowing more electrolytes for the redox reactions. This finding provides a new approach to enhancing the electrochemical performance of MXene in terms of specific capacitance and rate capability. Our results indicate that the optimal composition of MXene-C60 composite is 90% MXene +10% C60. However, it is important to note that the concentration of C60 particles needs to be carefully controlled since the capacitance decreases as the C60 concentration increases above 10%. Our study sheds light on the potential of MXene-C60 composites as high-performance electrode materials for supercapacitors. Future work could explore the use of other intercalating particles or optimize the composition of the MXene-C60 composite to further enhance its electrochemical performance. Overall, our findings contribute to the development of advanced energy storage devices that are crucial for a sustainable future.

4. SUMMARY AND CONCLUSIONS

In this study, we aimed to prepare MXene-C60 composites with different compositions and investigate the effect of interlayer spacing on the electrochemical properties of the composites. MXene was prepared by etching the MAX phase, and then, C60 and MXene composites were formed through a hydrothermal reaction and characterized through several techniques before using them to fabricate the electrode for a supercapacitor device. Our results show that the composite with a composition of 90% MXene +10% C60 exhibited the highest capacitance among all the composites studied. The

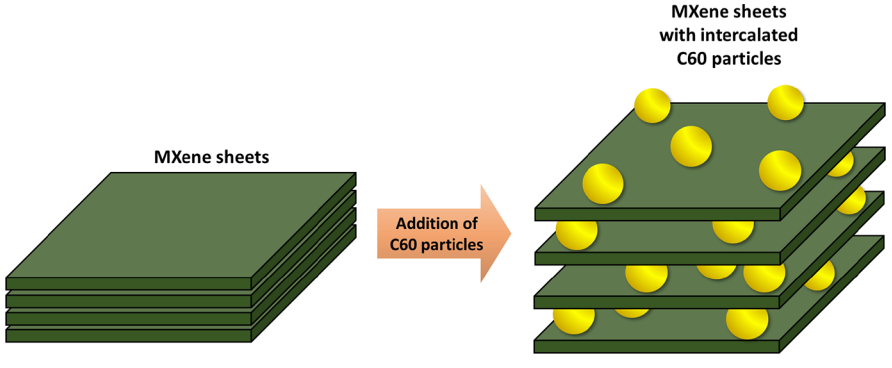

Figure 9. Schematic representation of C60 intercalation in the MXene layers.

https://doi.org/10.1021/acsomega.3c04058
ACS Omega 2024, 9, 227−238

increase in interlayer spacing achieved by intercalating C60 nanoparticles between MXene layers resulted in an improved capacitance and enhanced electrochemical performance of the composite. In summary, our work demonstrates that intercalation of C60 into MXene layers is a promising approach for enhancing the electrochemical properties of electrode materials for high-performance supercapacitor applications, which can have significant implications for the development of efficient energy storage systems.

■ ASSOCIATED CONTENT

Data Availability Statement

Data which supports plots in this paper is available from author on request.

■ AUTHOR INFORMATION

Corresponding Author

Saif Ullah Awan − *Department of Electrical Engineering, NUST College of Electrical and Mechanical Engineering, National University of Sciences and Technology (NUST), Islamabad 44000, Pakistan;* orcid.org/0000-0003-3370-3880; Email: saifullahawan@ceme.nust.edu.pk, ullahphy@gmail.com

Authors

Hassan Bukhari − *Department of Electrical Engineering, NUST College of Electrical and Mechanical Engineering, National University of Sciences and Technology (NUST), Islamabad 44000, Pakistan*

Asad M. Iqbal − *Department of Basic Sciences and Humanities, NUST College of Electrical and Mechanical Engineering, National University of Sciences and Technology (NUST), Islamabad 44000, Pakistan*

Danish Hussain − *Department of Mechatronics Engineering, NUST College of Electrical and Mechanical Engineering, National University of Sciences and Technology (NUST), Islamabad 44000, Pakistan*

Saqlain A. Shah − *Department of Physics, Forman Christian College (University), Lahore 54600, Pakistan*

Syed Rizwan − *Physics Characterization and Simulation Lab (PCSL), Department of Physics, School of Natural Sciences (SNS), National University of Sciences and Technology (NUST), Islamabad 44000, Pakistan;* orcid.org/0000-0002-6934-0949

Complete contact information is available at: https://pubs.acs.org/10.1021/acsomega.3c04058

Author Contributions

H.B. performed the experiments and data measurements and initial data analysis and completed his MS thesis. A.I. drafted the initial versions of manuscript and helped in preparations of figures, prepared Figures 1 and 9 completely with his own expertise. S.U.A. conceptualized the idea of project, helped in analyzing the data, data interpretation in detail, reviewed the manuscript, and played a leading role as supervisor. D.H. played his role during the review process and provided a lot of constructive feedback and prepared answers during the review process. He also prepared the figure we have used for the Graphical Abstract. S.S. contributed in drafting the manuscript and uplifted its English for the final version. S.R. cosupervised the project, provided the facilities, and helped in the process optimization and data analysis. All authors reviewed the final version of the manuscript.

Funding

The authors acknowledge the financial support from the Higher Education Commission of Pakistan under grant no. 5339/Federal/NRPU/R&D/HEC/2015 and project titled "Controlled Synthesis of Two-Dimensional Nanosheets and Multilayer For Electronic Devices"

Notes

The authors declare no competing financial interest.

■ REFERENCES

(1) Saikia, B. K.; Benoy, S. M.; Bora, M.; Tamuly, J.; Pandey, M.; Bhattacharya, D. A brief review on supercapacitor energy storage devices and utilization of natural carbon resources as their electrode materials. *Fuel* **2020**, *282*, 118796.

(2) Chen, Y.; Kang, Y.; Zhao, Y.; Wang, L.; Liu, J.; Li, Y.; Liang, Z.; He, X.; Li, X.; Tavajohi, N. A review of lithium-ion battery safety concerns: The issues, strategies, and testing standards. *J. Energy Chem.* **2021**, *59*, 83−99.

(3) Li, J.; Fleetwood, J.; Hawley, W. B.; Kays, W. From materials to cell: state-of-the-art and prospective technologies for lithium-ion battery electrode processing. *Chem. Rev.* **2022**, *122*, 903−956.

(4) Fan, L.; Tu, Z.; Chan, S. H. Recent development of hydrogen and fuel cell technologies: A review. *Energy Rep.* **2021**, *7*, 8421−8446.

(5) Zhao, J.; Burke, A. F. Review on supercapacitors: Technologies and performance evaluation. *J. Energy Chem.* **2021**, *59*, 276−291.

(6) Ferriday, T. B.; Middleton, P. H. Alkaline fuel cell technology-A review. *Int. J. Hydrogen Energy* **2021**, *46*, 18489−18510, DOI: 10.1016/j.ijhydene.2021.02.203.

(7) Ma, Y.; Xie, X.; Yang, W.; Yu, Z.; Sun, X.; Zhang, Y.; Yang, X.; Kimura, H.; Hou, C.; Guo, Z. Recent advances in transition metal oxides with different dimensions as electrodes for high-performance supercapacitors. *Adv. Compos. Hybrid Mater.* **2021**, 906−924.

(8) Zhou, Y.; Qi, H.; Yang, J.; Bo, Z.; Huang, F.; Islam, M. S.; Lu, X.; Dai, L.; Amal, R.; Wang, C. H. Two-birds-one-stone: multifunctional supercapacitors beyond traditional energy storage. *Energy Environ. Sci.* **2021**, *14*, 1854−1896.

(9) Liu, X.; Xu, F.; Li, Z.; Liu, Z.; Yang, W.; Zhang, Y.; Fan, H.; Yang, H. Y. Design strategy for MXene and metal chalcogenides/oxides hybrids for supercapacitors, secondary batteries and electro/photocatalysis. *Coord. Chem. Rev.* **2022**, *464*, 214544.

(10) Fu, W.; Turcheniuk, K.; Naumov, O.; Mysyk, R.; Wang, F.; Liu, M.; Kim, D.; Ren, X.; Magasinski, A.; Yu, M. Materials and technologies for multifunctional, flexible or integrated supercapacitors and batteries. *Mater. Today* **2021**, *48*, 176−197.

(11) Olabi, A. G.; Abbas, Q.; Al Makky, A.; Abdelkareem, M. A. Supercapacitors as next generation energy storage devices: Properties and applications. *Energy* **2022**, *248*, 123617.

(12) Xu, H.; Shen, M. The control of lithium-ion batteries and supercapacitors in hybrid energy storage systems for electric vehicles: a review. *Int. J. Energy Res.* **2021**, *45*, 20524−20544.

(13) Schütter, C.; Pohlmann, S.; Balducci, A. Industrial requirements of materials for electrical double layer capacitors: impact on current and future applications. *Adv. Energy Mater.* **2019**, *9*, 1900334.

(14) Li, T.; Ma, R.; Lin, J.; Hu, Y.; Zhang, P.; Sun, S.; Fang, L. The synthesis and performance analysis of various biomass-based carbon materials for electric double-layer capacitors: a review. *Int. J. Energy Res.* **2020**, *44*, 2426−2454.

(15) Kierzek, K.; Gryglewicz, G. Activated carbons and their evaluation in electric double layer capacitors. *Molecules* **2020**, *25*, 4255.

(16) Vicentini, R.; Da Silva, L. M.; Cecilio Junior, E. P.; Alves, T. A.; Nunes, W. G.; Zanin, H. How to measure and calculate equivalent series resistance of electric double-layer capacitors. *Molecules* **2019**, *24*, 1452.

(17) Chen, L.; Guo, M.; Deng, R.; Zhang, Q. Recent progress of Ni 3 S 2-based nanomaterials in different dimensions for pseudocapacitor application: synthesis, optimization, and challenge. *Ionics* **2021**, *27*, 4573−4618.

https://doi.org/10.1021/acsomega.3c04058
ACS Omega 2024, 9, 227−238

(18) Chodankar, N. R.; Pham, H. D.; Nanjundan, A. K.; Fernando, J. F.; Jayaramulu, K.; Golberg, D.; Han, Y. K.; Dubal, D. P. True meaning of pseudocapacitors and their performance metrics: asymmetric versus hybrid supercapacitors. *Small* **2020**, *16*, 2002806.
(19) Prasankumar, T.; Jose, J.; Jose, S.; Balakrishnan, S.P. Pseudocapacitors, in: *Supercapacitors for the Next Generation*; IntechOpen, 2021.
(20) Chen, R.; Yu, M.; Sahu, R. P.; Puri, I. K.; Zhitomirsky, I. The development of pseudocapacitor electrodes and devices with high active mass loading. *Adv. Energy Mater.* **2020**, *10*, 1903848.
(21) Chatterjee, D. P.; Nandi, A. K. A review on the recent advances in hybrid supercapacitors. *J. Mater. Chem. A* **2021**, *9*, 15880−15918.
(22) Sharma, K.; Arora, A.; Tripathi, S. K. Review of supercapacitors: Materials and devices. *J. Energy Storage* **2019**, *21*, 801−825.
(23) Zhang, Y.; Mei, H. x.; Cao, Y.; Yan, X. h.; Yan, J.; Gao, H. l.; Luo, H. w.; Wang, S. w.; Jia, X. d.; Kachalova, L.; Yang, J.; Xue, S. c.; Zhou, C. g.; Wang, L. x.; Gui, Y. h. Recent advances and challenges of electrode materials for flexible supercapacitors. *Coord. Chem. Rev.* **2021**, *438*, 213910.
(24) Lokhande, P. E.; Chavan, U. S.; Pandey, A. Materials and fabrication methods for electrochemical supercapacitors: overview. *Electrochem. Energy Rev.* **2020**, *3*, 155−186.
(25) Zhang, P.; Wang, F.; Yang, S.; Wang, G.; Yu, M.; Feng, X. Flexible in-plane micro-supercapacitors: progresses and challenges in fabrication and applications. *Energy Storage Mater.* **2020**, *28*, 160−187.
(26) Wang, Y.; Wu, X.; Han, Y.; Li, T. Flexible supercapacitor: overview and outlooks. *J. Energy Storage* **2021**, *42*, 103053.
(27) Xu, B.; Zhang, H.; Mei, H.; Sun, D. Recent progress in metal-organic framework-based supercapacitor electrode materials. *Coord. Chem. Rev.* **2020**, *420*, 213438.
(28) Attia, S. Y.; Mohamed, S. G.; Barakat, Y. F.; Hassan, H. H.; Zoubi, W. A. Supercapacitor electrode materials: Addressing challenges in mechanism and charge storage. *Rev. Inorganic Chem.* **2022**, *42*, 53−88.
(29) Singh, S.; Arka, G.N.; Gupta, S.; Prasad, S., Insights on a new family of 2D material mxene: A review, in: *AIP conference proceedings*; AIP Publishing LLC, 2021; pp. 040017.
(30) Zhang, Z.; Cai, Z.; Zhang, Y.; Peng, Y.; Wang, Z.; Xia, L.; Ma, S.; Yin, Z.; Wang, R.; Cao, Y.; Li, Z.; Huang, Y. The recent progress of MXene-Based microwave absorption materials. *Carbon* **2021**, *174*, 484−499.
(31) Pang, D.; Alhabeb, M.; Mu, X.; Dall'Agnese, Y.; Gogotsi, Y.; Gao, Y. Electrochemical actuators based on two-dimensional Ti3C2T x (MXene). *Nano Lett.* **2019**, *19*, 7443−7448.
(32) Zhan, X.; Si, C.; Zhou, J.; Sun, Z. MXene and MXene-based composites: synthesis, properties and environment-related applications. *Nanoscale Horiz.* **2020**, *5*, 235−258.
(33) Panda, S.; Deshmukh, K.; Khadheer Pasha, S. K.; Theerthagiri, J.; Manickam, S.; Choi, M. Y. MXene based emerging materials for supercapacitor applications: recent advances, challenges, and future perspectives. *Coord. Chem. Rev.* **2022**, *462*, 214518.
(34) Hu, M.; Zhang, H.; Hu, T.; Fan, B.; Wang, X.; Li, Z. Emerging 2D MXenes for supercapacitors: status, challenges and prospects. *Chem. Soc. Rev.* **2020**, *49*, 6666−6693.
(35) Chen, Y.; Yang, H.; Han, Z.; Bo, Z.; Yan, J.; Cen, K.; Ostrikov, K. K. MXene-based electrodes for supercapacitor energy storage. *Energy Fuels* **2022**, *36*, 2390−2406.
(36) Garg, R.; Agarwal, A.; Agarwal, M. A review on MXene for energy storage application: effect of interlayer distance. *Mater. Res. Express* **2020**, *7*, No. 022001.
(37) Simon, P. Two-dimensional MXene with controlled interlayer spacing for electrochemical energy storage. *ACS Nano* **2017**, *11*, 2393−2396.
(38) Tang, J.; Huang, X.; Qiu, T.; Peng, X.; Wu, T.; Wang, L.; Luo, B.; Wang, L. Interlayer space engineering of MXenes for electrochemical energy storage applications. *Chem. - Eur. J.* **2021**, *27*, 1921−1940.
(39) Lu, M.; Han, W.; Li, H.; Zhang, W.; Zhang, B. There is plenty of space in the MXene layers: The confinement and fillings. *J. Energy Chem.* **2020**, *48*, 344−363.
(40) Li, J.; Yuan, X.; Lin, C.; Yang, Y.; Xu, L.; Du, X.; Xie, J.; Lin, J.; Sun, J. Achieving high pseudocapacitance of 2D titanium carbide (MXene) by cation intercalation and surface modification. *Adv. Energy Mater.* **2017**, *7*, 1602725.
(41) Wudl, F. The chemical properties of buckminsterfullerene (C60) and the birth and infancy of fulleroids. *Acc. Chem. Res.* **1992**, *25*, 157−161.
(42) Ebbesen, T. W.; Tanigaki, K.; Kuroshima, S. Excited-state properties of C60. *Chem. Phys. Lett.* **1991**, *181*, 501−504.
(43) Arbogast, J. W.; Darmanyan, A. P.; Foote, C. S.; Diederich, F.; Whetten, R.; Rubin, Y.; Alvarez, M. M.; Anz, S. J. Photophysical properties of sixty atom carbon molecule (C60). *J. Phys. Chem.* **1991**, *95*, 11−12.
(44) Pan, Y.; Liu, X.; Zhang, W.; Liu, Z.; Zeng, G.; Shao, B.; Liang, Q.; He, Q.; Yuan, X.; Huang, D.; Chen, M. Advances in photocatalysis based on fullerene C60 and its derivatives: Properties, mechanism, synthesis, and applications. *Appl. Catal. B* **2020**, *265*, 118579.
(45) Diky, V. V.; Kabo, G. J. Thermodynamic properties of C60 and C70 fullerenes. *Russ. Chem. Rev.* **2000**, *69*, 95.
(46) Lichtenberger, D. L.; Wright, L. L.; Gruhn, N. E.; Rempe, M. E. Electronic structure and bonding of C60 to metals. *Synth. Metals* **1993**, *59*, 353−367.
(47) Forouzandeh, P.; Ganguly, P.; Dahiya, R.; Pillai, S. C. Supercapacitor electrode fabrication through chemical and physical routes. *J. Power Sources* **2022**, *519*, 230744.
(48) Vangari, M.; Pryor, T.; Jiang, L. Supercapacitors: review of materials and fabrication methods. *J. Energy Eng.* **2013**, *139*, 72−79.
(49) Choudhary, N.; Li, C.; Moore, J.; Nagaiah, N.; Zhai, L.; Jung, Y.; Thomas, J. Asymmetric supercapacitor electrodes and devices. *Adv. Mater.* **2017**, *29*, 1605336.
(50) Zhu, Z.; Tang, S.; Yuan, J.; Qin, X.; Deng, Y.; Qu, R.; Haarberg, G. M. Effects of various binders on supercapacitor performances. *Int. J. Electrochem. Sci.* **2016**, *11*, 8270−8279.
(51) Yang, G.-W.; Xu, C.-L.; Li, H.-L. Electrodeposited nickel hydroxide on nickel foam with ultrahigh capacitance. *Chem. Commun.* **2008**, 6537−6539.
(52) Mirghni, A. A.; Oyedotun, K. O.; Mahmoud, B. A.; Bello, A.; Ray, S. C.; Manyala, N. Nickel-cobalt phosphate/graphene foam as enhanced electrode for hybrid supercapacitor. *Composites, Part B* **2019**, *174*, 106953.
(53) Liu, F.; Yang, X.; Qiao, Z.; Zhang, L.; Cao, B.; Duan, G. Highly transparent 3D NiO-Ni/Ag-nanowires/FTO micro-supercapacitor electrodes for fully transparent electronic device purpose. *Electrochim. Acta* **2018**, *260*, 281−289.
(54) Salleh, N. A.; Kheawhom, S.; Hamid, N. A. A.; Rahiman, W.; Mohamad, A. A. Electrode polymer binders for supercapacitor applications: A review. *J. Mater. Res. Technol.* **2023**, 3470.
(55) Markevich, E.; Salitra, G.; Aurbach, D. Influence of the PVdF binder on the stability of LiCoO2 electrodes. *Electrochem. Commun.* **2005**, *7*, 1298−1304.
(56) Córdoba, J. M.; Sayagués, M. J.; Alcalá, M. D.; Gotor, F. J. Synthesis of Ti3SiC2 powders: reaction mechanism. *J. Am. Ceram. Soc.* **2007**, *90*, 825−830.
(57) Tang, K.; Wang, C.-a.; Huang, Y.; Xia, J. An X-ray diffraction study of the texture of Ti3SiC2 fabricated by hot pressing. *J. Eur. Ceramic Soc.* **2001**, *21*, 617−620.
(58) Tang, K.; Wang, C.-a.; Huang, Y.; Xu, X. Analysis on preferred orientation and purity estimation of Ti3SiC2. *J. Alloys Compds* **2001**, *329*, 136−141.
(59) Guo, Y.; Zhou, X.; Wang, D.; Xu, X.; Xu, Q. Nanomechanical properties of Ti3C2 mxene. *Langmuir* **2019**, *35*, 14481−14485.
(60) Sheng, X.; Zhao, Y.; Zhang, L.; Lu, X. Properties of two-dimensional Ti3C2MXene/thermoplastic polyurethane nanocomposites with effective reinforcement via melt blending. *Compos. Sci. Technol.* **2019**, *181*, 107710.

https://doi.org/10.1021/acsomega.3c04058
ACS Omega 2024, 9, 227−238

(61) Li, T.; Zhang, C.-Z.; Ding, D.; Fan, X.; Li, Y. Experimental and theoretical study on degradation of oxidized C60 in water via photo-Fenton method. *Chem. Eng. J.* **2018**, *334*, 587−597.
(62) Nath, S.; Pal, H.; Palit, D. K.; Sapre, A. V.; Mittal, J. P. Aggregation of fullerene, C60, in benzonitrile. *J. Phys. Chem. B* **1998**, *102*, 10158−10164.
(63) Xu, J.; Hu, X.; Wang, X.; Wang, X.; Ju, Y.; Ge, S.; Lu, X.; Ding, J.; Yuan, N.; Gogotsi, Y. Low-Temperature pseudocapacitive energy storage in Ti3C2Tx MXene. *Energy Storage Mater.* **2020**, *33*, 382−389.
(64) Boota, M.; Gogotsi, Y. MXene—conducting polymer asymmetric pseudocapacitors. *Adv. Energy Mater.* **2019**, *9*, 1802917.
(65) Girard, H.-L.; Wang, H.; d'Entremont, A.; Pilon, L. Physical interpretation of cyclic voltammetry for hybrid pseudocapacitors. *J. Phys. Chem. C* **2015**, *119*, 11349−11361.
(66) Gosser, D.K. *Cyclic voltammetry: simulation and analysis of reaction mechanisms*; VCH New York, 1993.
(67) Mashtalir, O.; Naguib, M.; Mochalin, V. N.; Dall'Agnese, Y.; Heon, M.; Barsoum, M. W.; Gogotsi, Y. Intercalation and delamination of layered carbides and carbonitrides. *Nat. Commun.* **2013**, *4*, 1716.
(68) Ramachandran, R.; Rajavel, K.; Xuan, W.; Lin, D.; Wang, F. Influence of Ti3C2Tx (MXene) intercalation pseudocapacitance on electrochemical performance of Co-MOF binder-free electrode. *Ceram. Int.* **2018**, *44*, 14425−14431.
(69) Li, J.; Wang, H.; Xiao, X. Intercalation in two-dimensional transition metal carbides and nitrides (MXenes) toward electrochemical capacitor and beyond. *Energy Environ. Mater.* **2020**, *3*, 306−322.
(70) Xu, J.; Peng, T.; Zhang, Q.; Zheng, H.; Yu, H.; Shi, S. Intercalation Effects on the Electrochemical Properties of Ti3C2T x MXene Nanosheets for High-Performance Supercapacitors. *ACS Appl. Nano Mater.* **2022**, *5*, 8794−8803.
(71) Simon, P.; Gogotsi, Y. Charge storage mechanism in nanoporous carbons and its consequence for electrical double layer capacitors. *Philos. Trans. R. Soc., A* **2010**, *368*, 3457−3467.
(72) Tan, J.; Li, Z.; Ye, M.; Shen, J. Nanoconfined Space: Revisiting the Charge Storage Mechanism of Electric Double Layer Capacitors. *ACS Appl. Mater. Interfaces* **2022**, *14*, 37259−37269.
(73) Burt, R.; Birkett, G.; Zhao, X. A review of molecular modelling of electric double layer capacitors. *Phys. Chem. Chem. Phys.* **2014**, *16*, 6519−6538.
(74) Jiang, Y.; Liu, J. Definitions of pseudocapacitive materials: a brief review. *Energy Environ. Mater.* **2019**, *2*, 30−37.
(75) Bhojane, P. Recent advances and fundamentals of Pseudocapacitors: Materials, mechanism, and its understanding. *J. Energy Storage* **2022**, *45*, 103654.
(76) Sinha, P.; Kar, K.K. Introduction to supercapacitors, in: *Handbook of Nanocomposite Supercapacitor Materials II: Performance;* Springer, 2020; pp 1−28.
(77) Sohan, A.; Banoth, P.; Aleksandrova, M.; Nirmala Grace, A.; Kollu, P. Review on MXene synthesis, properties, and recent research exploring electrode architecture for supercapacitor applications. *Int. J. Energy Res.* **2021**, *45*, 19746−19771.
(78) Nasrin, K.; Sudharshan, V.; Subramani, K.; Sathish, M. Insights into 2D/2D MXene heterostructures for improved synergy in structure toward next-generation supercapacitors: A review. *Adv. Funct. Mater.* **2022**, *32*, 2110267.
(79) Syamsai, R.; Grace, A. N. Ta4C3MXene as supercapacitor electrodes. *J. Alloys Compd.* **2019**, *792*, 1230−1238.
(80) Hart, J. L.; Hantanasirisakul, K.; Lang, A. C.; Anasori, B.; Pinto, D.; Pivak, Y.; van Omme, J. T.; May, S. J.; Gogotsi, Y.; Taheri, M. L. Control of MXenes' electronic properties through termination and intercalation. *Nat. Commun.* **2019**, *10*, 522.
(81) Kajiyama, S.; Szabova, L.; Sodeyama, K.; Iinuma, H.; Morita, R.; Gotoh, K.; Tateyama, Y.; Okubo, M.; Yamada, A. Sodium-ion intercalation mechanism in MXene nanosheets. *ACS Nano* **2016**, *10*, 3334−3341.
(82) Xu, J.; Peng, T.; Qin, X.; Zhang, Q.; Liu, T.; Dai, W.; Chen, B.; Yu, H.; Shi, S. Recent advances in 2D MXenes: preparation, intercalation and applications in flexible devices. *J. Mater. Chem. A* **2021**, *9*, 14147−14171.
(83) Xu, T.; Wang, Y.; Xue, Y.; Li, J.; Wang, Y. MXenes@ metal-organic framework hybrids for energy storage and electrocatalytic application: Insights into recent advances. *Chem. Eng. J.* **2023**, *470*, 144247.
(84) Li, J.; Sun, H.; Yi, S.-Q.; Zou, K.-K.; Zhang, D.; Zhong, G.-J.; Yan, D.-X.; Li, Z.-M. Flexible polydimethylsiloxane composite with multi-scale conductive network for ultra-strong electromagnetic interference protection. *Nano-Micro Letters* **2023**, *15*, 15.
(85) Li, J.; Wang, Y.; Song, H.; Guo, Y.; Hu, S.; Zheng, H.; Zhang, S.; Li, X.; Gao, Q.; Li, C.; Zhu, Z.; Wang, Y. Photocatalytic hydrogen under visible light by nitrogen-doped rutile titania graphitic carbon nitride composites: an experimental and theoretical study. *Adv. Compos. Hybrid Mater.* **2023**, *6*, 83.
(86) Li, J.; Wang, Y.; Li, X.; Gao, Q.; Zhang, S. A facile synthesis of high-crystalline g-C3N4 nanosheets with closed self-assembly strategy for enhanced photocatalytic H2 evolution. *J. Alloys Compd.* **2021**, *881*, 160551.
(87) Ammar, A. U.; Bakan-Misirlioglu, F.; Aleinawi, M. H.; Franzo, G.; Condorelli, G. G.; Yesilbag, F. N. T.; Yesilbag, Y. O.; Mirabella, S.; Erdem, E. All-in-one supercapacitors with high performance enabled by Mn/Cu doped ZnO and MXene. *Mater. Res. Bull.* **2023**, *165*, 112334.
(88) Ammar, A. U.; Yildirim, I. D.; Bakan, F.; Erdem, E. ZnO and MXenes as electrode materials for supercapacitor devices. *Beilstein J. Nanotechnol.* **2021**, *12*, 49−57.
(89) Dwivedi, N.; Dhand, C.; Kumar, P.; Srivastava, A. Emergent 2D materials for combating infectious diseases: The potential of MXenes and MXene−graphene composites to fight against pandemics. *Mater. Adv.* **2021**, *2*, 2892−2905.
(90) Liu, T.; Liu, X.; Graham, N.; Yu, W.; Sun, K. Two-dimensional MXene incorporated graphene oxide composite membrane with enhanced water purification performance. *J. Membr. Sci.* **2020**, *593*, 117431.
(91) Bao, Z.; Lu, C.; Cao, X.; Zhang, P.; Yang, L.; Zhang, H.; Sha, D.; He, W.; Zhang, W.; Pan, L.; Sun, Z. Role of MXene surface terminations in electrochemical energy storage: A review. *Chin. Chem. Lett.* **2021**, *32*, 2648−2658.
(92) Su, X.; Zhang, J.; Mu, H.; Zhao, J.; Wang, Z.; Zhao, Z.; Han, C.; Ye, Z. Effects of etching temperature and ball milling on the preparation and capacitance of Ti3C2MXene. *J. Alloys Compd.* **2018**, *752*, 32−39.
(93) Zhou, C.; Zhao, X.; Xiong, Y.; Tang, Y.; Ma, X.; Tao, Q.; Sun, C.; Xu, W. A review of etching methods of MXene and applications of MXene conductive hydrogels. *Eur. Polym. J.* **2022**, *167*, 111063.
(94) Guo, J.; Peng, Q.; Fu, H.; Zou, G.; Zhang, Q. Heavy-metal adsorption behavior of two-dimensional alkalization-intercalated MXene by first-principles calculations. *J. Phys. Chem. C* **2015**, *119*, 20923−20930.
(95) Ye, M.; Wang, X.; Liu, E.; Ye, J.; Wang, D. Boosting the photocatalytic activity of P25 for carbon dioxide reduction by using a surface-alkalinized titanium carbide MXene as cocatalyst. *ChemSusChem* **2018**, *11*, 1606−1611.
(96) Tian, Y.; An, Y.; Feng, J. Flexible and freestanding silicon/MXene composite papers for high-performance lithium-ion batteries. *ACS Appl. Mater. Interfaces* **2019**, *11*, 10004−10011.
(97) Aslam, M. K.; Xu, M. A Mini-Review: MXene composites for sodium/potassium-ion batteries. *Nanoscale* **2020**, *12*, 15993−16007.
(98) Zhao, M. Q.; Ren, C. E.; Ling, Z.; Lukatskaya, M. R.; Zhang, C.; Van Aken, K. L.; Barsoum, M. W.; Gogotsi, Y. Flexible MXene/carbon nanotube composite paper with high volumetric capacitance. *Adv. Mater.* **2015**, *27*, 339−345.
(99) Qian, K.; Li, S.; Fang, J.; Yang, Y.; Cao, S.; Miao, M.; Feng, X. C60 intercalating Ti3C2Tx MXenes assisted by γ-cyclodextrin for electromagnetic interference shielding films with high stability. *J. Mater. Sci. Technol.* **2022**, *127*, 71−77.

https://doi.org/10.1021/acsomega.3c04058
ACS Omega 2024, 9, 227−238